One-way membrane trafficking of SOS in receptor-triggered Ras activation

Sune M. Christensen[1,§,†], **Hsiung-Lin Tu**[1,‡,†], **Jesse E. Jun**[2,†], **Steven Alvarez**[1], **Meredith G. Triplet**[1], **Jeffrey S. Iwig**[3], **Kamlesh K. Yadav**[4,¶], **Dafna Bar-Sagi**[4], **Jeroen P. Roose**[2,#,*], and **Jay T. Groves**[1,#,*]

[1]Department of Chemistry, University of California, Berkeley, California, USA

[2]Department of Anatomy, University of California, San Francisco, California, USA

[3]Howard Hughes Medical Institute, Department of Molecular and Cell Biology, University of California, Berkeley, California, USA

[4]Department of Biochemistry, New York University School of Medicine, New York, USA

Abstract

SOS is a key activator of the small GTPase Ras. In cells, SOS-Ras signaling is thought to be initiated predominantly by membrane-recruitment of SOS via the adaptor Grb2 and balanced by rapidly reversible Grb2:SOS binding kinetics. However, SOS has multiple protein and lipid interactions that provide linkage to the membrane. In reconstituted membrane experiments, these Grb2-independent interactions are sufficient to retain SOS on the membrane for many minutes, during which a single SOS molecule can processively activate thousands of Ras molecules. These observations raise questions concerning how receptors maintain control of SOS in cells and how membrane-recruited SOS is ultimately released. We addressed these questions in quantitative reconstituted SOS-deficient chicken B cell signaling systems combined with single molecule measurements in supported membranes. These studies reveal an essentially one-way trafficking

Contact: To whom correspondence should be addressed: jeroen.roose@ucsf.edu or jtgroves@lbl.gov.
§Present address: Novozymes A/S, Bagsvaerd, Denmark.
‡Present address: Institute for Molecular Engineering, University of Chicago, Chicago, Illinois, USA
¶Present address: Department of Urology Icahn School of Medicine at Mount Sinai, New York, USA
†These authors contributed equally to this work.
#These authors jointly supervised this work.

Note: Supplementary information including 8 figures, 7 Supplementary Notes and a movie is available online.

Code availability

Supplementary Note 7 provides a detailed account of employed data analysis procedures which can be implemented in a given coding language.

Author contributions

S.M.C., H.L.T., J.E.J. performed experiments and analyzed data. S.A., M.G.T. assisted with live cell experiments. J.I. purified proteins. K.K.Y. performed COS1 cell experiments under supervision of D.B.-S.. J.T.G., J.P.R., S.M.C., H.L.T., J.E.J. conceptualized and designed experiments. S.M.C., H.L.T., J.E.J., J.P.R. & J.T.G. wrote the paper. J.T.G., J.P.R. supervised the project. All authors discussed and commented on the results.

process in which membrane-recruited SOS remains trapped on the membrane and continuously activates Ras until it is actively removed via endocytosis.

Introduction

Ras is a membrane-anchored small GTPase that plays a central role in many signaling pathways. Ras can exist in an inactive (GDP-bound) or active (GTP-bound) state. Ras activation is mediated by a variety of Ras guanine nucleotide exchange factors (RasGEFs) that catalyze the exchange of Ras-bound nucleotide with cytoplasmic GTP[1–3]. This process is opposed by Ras GTPase-activating proteins (RasGAPs) that enhance the intrinsic GTPase activity of Ras and thus promote Ras deactivation[1]. Ras activation must be tightly regulated; aberrant activation of Ras is responsible for many human cancers[4].

Son of Sevenless (SOS) is a widely distributed RasGEF[5–7] and full activation of SOS through an allosteric mechanism results in digital patterns of receptor-induced Ras-kinase signaling[8,9]. The activation of Ras by SOS is critical for diverse processes such as cell growth[10], T cell activation and development[8,9,11,12], early B cell development[13], embryogenesis[14], and differentiation of embryonic stem cells[15].

Receptor-triggered activation of SOS is a multilayered process involving membrane recruitment, release of autoinhibition, and allosteric modulation by Ras. The initial membrane recruitment of SOS is thought to occur via association of PxxP motifs in the C-terminal proline-rich (PR) domain with Grb2, which in turn binds phospho-tyrosine motifs on activated receptors or transmembrane adaptor proteins[6,7,10,16–21]. SOS additionally contains a series of N-terminal domains with homology to Dbl (DH) and Pleckstrin (PH) as well as a Histone Fold (HF) domain (Fig. 1a), which can autoinhibit SOS activity when assayed in solution. On membranes, this autoinhibition is released through interactions with various membrane lipids[22–24] (reviewed in ref.[9]). Full activation of SOS is contingent on binding of Ras to an allosteric pocket situated at the rim of the REM and CDC25 domains[25]. The REM and CDC25 domains in SOS1 together form the catalytic core, which we term SOS^{Cat} throughout the manuscript (Fig. 1a). Mutations in *SOS1* that perturb these regulatory functions result in altered signaling behavior and have been implicated in developmental disorders such as Noonan[26], Costello and CFC-syndrome[27]. SOS2 has a very similar domain make-up, but appears somewhat redundant to SOS1 in cells[13]; in this study we solely focus on SOS1.

Historically, SOS activation was rationalized in terms of a simple membrane recruitment model based on substrate accessibility (Fig. 1b). Grb2 binding to activated receptors recruits SOS–Grb2 complex from the cytosol, thereby positioning SOS in proximity to membrane-anchored Ras and thus promoting nucleotide exchange[5,28]. However, the importance of Grb2-mediated membrane recruitment is challenged by observations that truncated SOS constructs lacking the PR domain still localize to the membrane upon receptor stimulation and are fully signaling competent, or even exhibit increased responsiveness, relative to the full length enzyme[29–34]. Recent work with mouse embryonic stem cells (mESC)[15] demonstrated that, besides Grb2-facilitated membrane recruitment, SOS activity is governed by summation of weak to moderate protein-protein and protein-lipid interactions mediated

by the multiple domains of SOS[15,24,33,35]. These studies imply that the recruitment to membrane integral receptors via Grb2 is an oversimplified model for SOS function (see also Supplementary Note 1).

We have observed that SOS constructs, lacking the Grb2-binding PR domain, are successfully recruited to reconstituted Ras functionalized membranes through Ras- and lipid-binding interactions. Additionally, a single SOS molecule has the capacity to processively activate thousands of Ras proteins during a single membrane residency period (Fig. 1c,d). This finding was realized using a micropatterned fluid supported lipid bilayer platform[36,37] in which the catalytic activity of individual SOS molecules can be directly resolved[38]. Such high degrees of processivity and essentially irreversible membrane recruitment in the activation of Ras by SOS are not captured in earlier mechanistic and computational models of SOS activity, or in synthetic biology approaches using Grb2–SOS1 fusion proteins[8,15]. The question if such extreme processivity of SOS occurs in cells arises immediately, and if so, how is it being regulated?

To address this question we mapped the individual contributions of the different domains in SOS1 to membrane association through a series of single molecule dwell time measurements and bulk kinetic observations. These studies utilized a reconstituted membrane system in combination with quantitative cell-based signaling assays (for more details see Supplementary Note 1). Altogether, our results reveal an essentially one-way trafficking process in which membrane-recruited SOS1 remains trapped on the membrane and continuously activates Ras until it is actively removed, such as by endocytosis. This mechanism differs substantially from the reversible Grb2 dependent process that has been generally assumed[6,7,10,16–19]. The Ras activation machinery can remain active or be inactivated irrespective of the triggering state of the receptor that initiated the signal. This significantly impacts the quantitative input-response function for Ras activation by receptor triggering and underscores the importance of strong inhibition of spontaneous SOS activation.

Results

Supported lipid bilayer SOS activation assay

We developed an imaging assay to study the interaction of SOS with Ras on Supported Lipid Bilayers (SLBs, Fig. 2a). In this experimental configuration, H-Ras (1–181, C118S) (henceforth referred to as Ras) was coupled at C181 to the bilayer via a maleimide functionalized lipid (online Methods), yielding permanently bound and laterally mobile Ras that is fully functional with respect to SOS activity[22,38,39] (Supplementary Fig. 1a). A calibration curve obtained using fluorescence correlation spectroscopy (FCS) provided access to the local surface density of Ras via epifluorescence imaging of Ras-bound fluorescent nucleotide labels (GDP- and GTP-BODIPY, Supplementary Fig. 1b and ref.[38]). Labeling of SOS with a photostable and bright fluorophore (ATTO 647N) facilitated reliable counting and tracking of individual SOS molecules at the membrane surface by total internal reflection fluorescence microscopy (TIRFM). Control experiments showed that labeling did not perturb the observed activity of SOS (Supplementary Fig. 1c).

In this system, measurements are intiated by flowing purified SOS1 over the Ras functionalized SLBs in a transient pulse with a defined concentration profile (Fig. 2a, left). During such a pulse, SOS1 interacts with membrane-bound Ras and, in the absence of free nucleotide in solution, becomes trapped upon binding Ras at the catalytic site[30,40]. This provided a convenient way of quantifying the probability of SOS1 engaging Ras by directly counting the number of SOS1 molecules remaining at the bilayer after a pulse (Fig. 2b and online Methods). Chasing with unlabeled nucleotide initiated the exchange reaction and resulted in processive (i.e., sustained) turnover of Ras by the recruited and successfully activated SOS1 molecules (Fig. 2a, right, and Supplementary Fig. 1d). A constant flow during the experiment ensured that dissociated SOS1 was removed from the reaction chamber, thus permitting measurement of desorption kinetics.

Allosteric activation of SOS via altered membrane recruitment

An important functional aspect of SOS1 in the cellular context is its activation by RasGTP binding to an allosteric site, located between the CDC25 and Ras exchanger motif (REM) domains in the catalytic core termed SOS[Cat25]. This allosteric activation depends sensitively on the nucleotide state of Ras[41] and is thought to enable a RasGTP positive-feedback loop operating at the membrane[8,9].

Allosteric binding of Ras by SOS also provides an alternate mechanism to recruit SOS to the membrane. Here, we first quantitatively analyzed recruitment by examining the SOS[Cat] module that harbors both the active site and the allosteric Ras binding pocket, but lacks any lipid binding domains[25]. SOS[Cat] was recruited to the Ras bilayer during the pulse phase of the assay (Fig. 2c). The known concentration profile of SOS[Cat] during the pulse combined with locally measured Ras densities permitted quantitating the recruitment probability from the adsorption traces (i.e., the probability that a SOS[Cat] molecule gets trapped upon collision with Ras at the membrane (Fig. 2d and online Methods)).

We found that membrane recruitment of SOS[Cat] was sensitive to the nucleotide state of Ras with ~16 fold enhancement on SLBs displaying RasGTP (Fig. 2d). A Y64A point mutation in Ras, previously shown to abolish Ras binding to the catalytic site of SOS[42], resulted in only transient recruitment of SOS[Cat], demonstrating that, as expected, SOS is trapped at the membrane upon binding Ras at the catalytic site in the absence of free nucleotide (Fig. 2c). Nucleotide-dependent recruitment was preserved for Ras[Y64A], indicating that the allosteric binding pocket is the primary determinant for this property of SOS[Cat] (Fig. 2d). A W729E point mutation in SOS1, known to prevent binding of allosteric Ras[8,43], essentially abrogated recruitment (Fig. 2c,d). Upon chasing with nucleotide, a population of highly processive SOS[Cat] remained at the membrane (Fig. 2c, note the tail of the curve), which we identify as successfully activated SOS[Cat] molecules. The long-lived (minute to hour scale) membrane-bound SOS[Cat] was catalytically active (Supplementary Fig. 1d and ref.[38]), indicating that release of SOS from the membrane was predominantly limited by the allosterically bound Ras.

We substantiated our findings in the SLB experiments with cellular assays (see Supplementary Note 2 and Supplementary Fig. 2a–d). Collectively, the data demonstrate a very distinct positive allosteric effect of RasGTP at the stage of membrane recruitment.

These results, taken together with the insensitivity of the average specific activity of SOS to the nucleotide state of Ras[38], indicate that RasGTP-mediated recruitment of SOS via its allosteric site is one mechanism by which the well-known accelerating effect of RasGTP on SOS mediated Ras activation is achieved (commonly referred to as positive feedback)[8,22,41].

Regulation of membrane binding by N-terminal domains

It is not known if membrane recruitment and retention of SOS^{Cat} are influenced by its flanking lipid-binding domains. At the N-terminal side, the catalytic core of SOS1 is flanked by a DH-PH cassette and a HF domain (Fig. 3a). Structural and biochemical studies have shown that the N-terminal domains exert an autoinhibitory effect on SOS1 activity, presumably through steric obstruction of the allosteric Ras binding pocket as observed in crystal structures[23,43]. The PH domain interacts with phosphatidylinositol 4,5-bisphosphate (PiP_2) lipids[35,44] and phosphatidic acid (PA)[33] and the HF domain harbors several additional interaction sites for negatively charged lipids[23,24]. These lipid interactions are generally believed to play a role in the release of autoinhibition, but the underlying mechanisms are at this stage unclear.

We observed a pronounced damping effect on initial membrane recruitment of SOS1 upon adding the N-terminal domains to SOS^{Cat}. Appending the DH-PH unit to the catalytic core (SOS^{DPC}) reduced recruitment to the membrane by ~3 fold. Inclusion of the full N-terminus (construct comprising HF-DH-PH-Cat domains (SOS^{HDPC})) damped recruitment ~66 fold relative to SOS^{Cat} (Fig. 3b). Even in the case of the highly autoinhibited HDPC construct, Ras-specific binding was evident (Supplementary Fig. 2e). These observations clearly demonstrate that a major property of the N-terminus is to down-modulate spontaneous SOS1 activation by hindering its initial recruitment to the membrane, consistent with the steric hindrance of the allosteric Ras binding site observed in structures[23,43]. Interestingly, a gain of function R552G point mutation associated with Noonan syndrome $(SOS^{HDPC(R552G)})$[26] caused a slight relief of such inhibition compared to SOS^{HDPC} (Fig. 3b and Supplementary Fig. 3a), emphasizing the importance of a tightly regulated membrane recruitment step. As observed for SOS^{Cat} (Fig. 2c,d), the longer constructs also exhibited increased recruitment on bilayers displaying RasGTP (Supplementary Fig. 3a).

Although the N-terminal domains inhibited initial recruitment, SOS^{DPC} and SOS^{HDPC} exhibited extremely long dwell times on Ras functionalized bilayers (mean residency period in the hour scale, Fig. 3c, Supplementary Fig. 3b,c and online Methods). The N-terminal domains thus mediate two major functions: inhibition of initial recruitment probability and enhancement of the dwell time in the active membrane bound state. This anti-correlation between membrane recruitment probability and dwell time gives rise to an interesting dual functionality where rare activation events are coupled to a potent response (Supplementary Fig. 3d,e).

Multi-component analysis of SOS-Ras-ERK signaling

To establish the impact of intrinsic chemical SOS1 properties—as determined from reconstituted SLB assays—on cellular SOS1-Ras signaling, we optimized a SOS1 and SOS2 double-deficient $(SOS1^-2^-)$ DT40 chicken B cell system that we used previously to

characterize digital SOS1-Ras-MAPK ERK signal transduction upon B cell receptor (BCR) ligation[8,45,46]. Here, we introduced EGFP-tagged variants of human SOS1 (hSOS1) into these cells that are entirely devoid of endogenous SOS1–2, left cells unstimulated or induced BCR ligation, and monitored EGFP-SOS localization by fluorescence microscopy or activation of the ERK kinase using a phospho-ERK (pERK) antibody by flow cytometry[8,46] (Fig. 4a,b). Henceforth, we shall refer to the latter experimental platform as the p-FLOW assay (online Methods). This assay reveals the quantitative magnitudes of Ras-ERK responses at the individual cell level along with SOS1 expression levels. Figure 4c,d display 3D representations of such data mapping the time evolution of pERK after BCR stimulation as a function of SOS1 expression level. pERK traces corresponding to specific SOS1 levels represent two-dimensional slices through the data (Fig. 4f,g and 4i,j).

Timely signaling requires SOS^{Cat}-flanking domains

Transient transfection of EGFP-tagged full-length human SOS1 (SOS^{FL}) rescued characteristic BCR-induced pERK patterns in SOS-deficient DT40 cells (Fig. 4b and Supplementary Fig. 4a,b). SOS^{Cat}, lacking the Grb2-binding domain as well as the N-terminal lipid-interacting domains, triggered Ras-ERK signaling patterns that differed substantially from those triggered by SOS^{FL} (Fig. 4c,d and Supplementary Fig. 4c,d). Cells expressing high levels of SOS^{Cat} exhibited more spontaneous activation of ERK in the absence of receptor stimulation than those with SOS^{FL} (Fig. 4e,h). Even under these conditions, BCR stimulation further increased ERK activation in SOS^{Cat} containing cells (Fig. 4c,f,i). Another notable difference was the signal attenuation. While SOS^{FL}-induced pERK signals decreased at later time points following BCR stimulation (10–20 min.), SOS^{Cat} continued to signal in a sustained manner and SOS^{Cat} outperformed SOS^{FL} (Fig. 4f,i). The sustained signaling from SOS^{Cat} cells suggests the essentially irreversible membrane anchoring of SOS^{Cat} observed in reconstituted assays may exist in cells as well, but not for SOS^{FL}.

At first glance, domains flanking SOS^{Cat} might appear to merely dampen signal output. However, selective examination of cells expressing intermediary SOS levels revealed SOS^{FL} signaled more efficiently than SOS^{Cat} in response to BCR stimulation (Fig. 4g,j). Moreover, this intermediary SOS^{FL} level resulted in rescue of pERK responses that were near identical to those observed for wild type DT40 cells, arguing that reconstitution with intermediary hSOS1 level matches the physiological level expressed in WT DT40 cells (Supplementary Fig. 4b). The data reveal that domains flanking SOS^{Cat} have both positive- and negative-regulatory roles.

SOS autoinhibition prevents spontaneous activation

A number of structural and cellular studies established regulatory mechanisms that impact SOS1 activity, but several proposed mechanisms appear contradictory[22–24,43]. To understand how SOS1 restricts spontaneous signaling in cells yet allows for controlled allosteric activation near the membrane interface, we first focused on SOS^{Cat}-flanking domains in the basal state (Fig. 5a–c), i.e., in resting cells[6,7].

Addition of N-terminal domains to SOS^{Cat} blocked the spontaneous activation of Ras-ERK in cells expressing high levels of SOS (Fig. 5a,b and Supplementary Fig. 5a–d). The inhibitory potential scales in an incremental manner with the number of domains flanking the catalytic core; i.e., SOS^{DPC} signaling is more restrained than SOS^{Cat} (Fig. 5a) and SOS^{HDPC} is more inhibited than SOS^{DPC} (Fig. 5b). These results corroborate the supported bilayer results in Figure 3b. Structural and biochemical studies on SOS1 demonstrated that the DH domain limits Ras-binding at the allosteric pocket and without removal of DH-mediated auto-inhibition and allosteric activation, the catalytic pocket cannot fully accommodate RasGDP nor dislodge GDP from Ras[22,43]. The HF strengthens SOS autoinhibition by blocking allosteric activation and by stabilizing a closed conformation of SOS[23,47]. These structural findings agree with our p-FLOW results for the resting cell state (Fig. 5a–c). Of note, despite considerable effort, it has not been feasible to purify functional full-length SOS1 that includes the PR domain, preventing its examination in our earlier SLB assays[38].

The C-terminal PR domain is most noted for its positive regulatory role in connecting SOS to activated receptors via Grb2. Grafting only the PR domain onto SOS^{Cat} revealed an inhibitory effect of this domain in restricting ligand-independent activation of SOS1 (Fig. 5c) that is independent of the autoinhibitory effect of the HF and DH-PH domains. The magnitude of inhibition conferred by the PR domain is comparable to that of the DH-PH domain relative to SOS^{Cat} (Fig. 5a,c), demonstrating that the N- and C-terminal domains bestow similar potency to curb activity from the catalytic SOS^{Cat} core in resting cells.

Positive regulation of SOS activity in stimulated cells

Next we investigated SOS1 regulation in BCR-stimulated cells expressing intermediary SOS1-EGFP levels (Fig. 5d–f). It has been reported that autoinhibition by the DH domain can be released by electrostatic interaction of the PH domain with membrane lipids, allowing allosteric Ras binding[15,22,33]. In our p-FLOW assay we found that the DH-PH domain alone had a purely inhibitory effect relative to SOS^{Cat} under conditions of BCR stimulation (Fig. 5d). Contrasting the addition of the DH-PH appendage, inclusion of the HF domain to SOS^{DPC} resulted in increased signaling output (Fig. 5e). The positive regulatory role of HF after BCR stimulation was also observed for SOS containing the PR domain (Supplementary Fig. 5e–g). These findings are in agreement with the *in vitro* observation that HF enhances the residence time of membrane recruited SOS (Fig. 3c).

For the DH-PH, our result from stimulated cells conflicted with the increased dwell time observed in the SLB assays (Fig 3c). The inhibitory effect of DH-PH is surprising because PH-lipid interaction has been reported to positively regulate GTP loading of Ras in COS-1 cells and in mouse embryonic stem cell differentiation[15,22,33]. This disparity may arise from the HF truncation counteracting the phospholipid binding of PH in the cell system. To test this, combined mutation of K456E and R459E (KR-EE mutation) was introduced within the PH domain, disrupting PI(4,5)P$_2$-PH interaction[15,35] and BCR-stimulated ERK activation was compared to wild-type SOS1 variants (Fig. 5g–i). The KR-EE mutation in DPC format had relatively small impact, resulting in a small decrease in pERK (Fig. 5g). However, KR-EE mutation in HDPC markedly antagonized SOS1 activation throughout the entire assay

duration, supporting the requirement of HF to stabilize membrane-targeted SOS1 through phospholipid-PH interaction[24] (Fig. 5h). The KR-EE HDPC signals comparable to the shorter WT DPC, negating the positive regulatory effect of HF domain (Fig. 5i). These observations collectively indicate that lipid interaction through HF and PH domains co-operate to stabilize active SOS1 at the membrane.

In sum, p-FLOW results presented in Figure 5 combined with single molecule measurements in our SLB assays (Fig. 2,3) indicated that the flanking domains on both sides of SOS^{Cat} have evolved to simultaneously dampen SOS activity in the basal state but enhance SOS activity upon receptor stimulation (further discussed in Supplementary Note 3).

Regulation of super-processive SOS by endocytosis

SOS^{Cat}, SOS^{DPC}, and SOS^{HDPC} are all highly processive in SLB assays and less sensitive to attenuation at late time points of induced signaling in cellular p-FLOW assays when compared to SOS^{FL}. Interestingly, full-length (SOS^{FL}) mimics these characteristics of SOS truncations when functionalized with a C-terminally grafted farnesylation signal sequence from H-Ras, which artificially targets SOS1 to the membrane (Supplementary Fig. 6)[48]. Deletion of the Grb2-binding domain of SOS1, its putative primary mode of membrane recruitment, thus produces a molecular and cellular phenotype resembling artificial membrane targeting.

To further investigate membrane recruitment and subsequent trafficking of SOS1, we imaged SOS1-EGFP in living cells by TIRFM and spinning disc confocal microscopy. For this experiment, we employed the hybrid live cell-supported bilayer platform[49–52] to simulate the native signaling geometry of B cells interacting with antigen presenting cells (Supplementary Fig. 7a). SOS-deficient DT40 B cells expressing human SOS1-EGFP were spread on SLBs functionalized with antibody that recognizes and activates the BCR[53], in turn triggering activation of SOS[54,55] (online Methods).

B cell activation from the supported membrane led to formation of BCR microclusters, here observed by TIRFM imaging of a Cy5 label on the antibody (Fig. 6a). SOS^{FL} was efficiently recruited to sites of BCR clusters whereas SOS^{Cat} did not colocalize with BCR clusters although it localizes to the membrane, presumably on the basis of binding to allosteric Ras (Fig. 6a,b). SOS^{HDPC} also lacked colocalization with the BCR clusters (Fig. 6b and Supplementary Fig. 7b). Contrasting reports have addressed the role of signaling complexes and SOS1 function. In our B cell system devoid of any endogenous SOS expression, chimeric SOS^{HDPC}-SH2, with a single SH2 domain of Grb2 grafted onto SOS^{HDPC}, did not colocalize with sites of BCR microclusters (Fig. 6b and Supplementary Fig. 7b). Conversely, addition of the PR domain to SOS^{Cat} or to SOS^{DPC} enabled SOS1-BCR colocalization (Fig. 6b, Supplementary Fig. 7b, Supplementary Note 4).

Over time, the initially scattered BCR clusters concatenated and moved toward the center of the synapses formed between the B cells and the SLB. About 15–20 minutes after cell landing, a large central cluster appeared, a phenomenon commonly referred to as 'BCR capping'[56] (Fig. 6c and Supplementary Movie 1). SOS^{FL} initially moved with the activated

BCR, but at later time points we found that it was depleted from the central BCR cluster (Fig. 6d,e). Thus, SOS^{FL} leaves the plasma membrane at the site of the central BCR cluster, which also correlates with attenuation of SOS^{FL}-driven Ras-ERK signaling at later time points (Fig. 4g). Confocal fluorescence microscopy revealed the appearance of punctate SOS structures located inside the cells, reminiscent of endocytic vesicles (Fig. 7a). Moreover, these vesicle-like structures appeared only for SOS^{FL} but not for SOS^{HDPC} or the chimeric SOS^{HDPC}–SH2 and only on bilayers displaying the BCR activating antibody (Fig. 7a,b). These observations suggest that removal of SOS1 from the membrane in a BCR signal dependent process requires the C-terminus.

To more definitively address disappearance of SOS^{FL} from the plasma membrane, we utilized COS-1 cells with a much larger cytoplasm compared to DT40 B cells. Visualizing transfected, EGFP-tagged SOS^{FL} revealed predominantly cytoplasmic and evenly distributed SOS1 prior to EGF (Epidermal Growth Factor) stimulation. We observed prominent membrane-recruitment of SOS1 at the plasma membrane 10 min. after EGF stimulation. By 30 min post-stimulation, most SOS molecules localized to perinuclear, vesicular structures (Fig. 7c). The vesicular SOS1 colocalized with the early endosomal marker protein Rab5[57], indicating that SOS1 molecules are removed from the plasma membrane via endocytosis (Fig. 7d). We found that the kinetics of SOS1 endocytosis were influenced by the allosteric Ras binding pocket. A SOS1 mutant impaired in allosteric Ras binding (SOS$^{FL-L687E\ R688A}$) exhibited accelerated endocytosis (Fig. 7e). Binding of SOS1 to Ras via its allosteric pocket thus appears to counteract endocytosis of SOS1.

Discussion

Signal propagation from receptors to the Ras pathway is commonly accepted to involve recruitment of SOS from the cytosol to the plasma membrane via the adaptor protein Grb2. In its classical interpretation, the increased membrane localization of SOS is presumed to tip the RasGEF-RasGAP balance at the membrane in favor of Ras activation, thus explaining how signals are relayed downstream. However, several results have challenged this classical model, led by the recurring observation that SOS truncations lacking the Grb2-binding PR domain remain signaling competent in cells[29–34]. More recently, we have shown that SOS can stably associate with a lipid membrane surface by engaging Ras at the allosteric binding pocket. In reconstituted membrane systems, this mechanism alone (i.e., independent of other mechanisms of SOS membrane anchoring) is sufficient for sustained association of SOS with the membrane where it can processively activate thousands of Ras molecules[38]. Strikingly, essentially no dynamic equilibrium is observed; membrane recruitment of SOS is quasi-irreversible at signaling relevant timescales.

Here we have demonstrated that membrane recruitment probability of SOS by allosteric Ras is strongly accelerated by RasGTP relative to RasGDP. This explains how SOS constructs lacking the Grb2 binding PR domain are capable of sensing receptor triggering. In a cellular context RasGTP levels are primed following receptor activation, e.g., due to the activity of RasGRP or other exchange factors, which will produce RasGTP and ignite SOS recruitment, fuelled by strong positive feedback as recruited SOS produces increasingly more RasGTP. This ability to respond to receptor stimuli, independently of Grb2, is further augmented by

the lipid interacting PH and HF domains that bind lipidic second messengers such as PiP_2 and PA.

In light of the spontaneous and nearly irreversible activating characteristics of SOS, the question shifts to how receptor-mediated signals maintain control of SOS via Grb2 binding. The literature abounds with apparently conflicting results on this matter. In particular, it has been unclear whether the C-terminal PR domain plays a positive, redundant or even negative regulatory role in SOS signaling. Our p-FLOW assay, which considers the multi-factorial aspects of signal transduction (i.e., expression level, pathway activity and time after receptor stimulation), revealed that the PR domain performs dual functions in receptor-stimulated cells, acting as a signal facilitator or signal terminator, depending on the phase of the signaling process. In addition, the PR domain contributes to inhibition of SOS in the basal state.

From the perspective of receptor-mediated activation of SOS, Grb2 binding by the PR domain clearly increases the rate of activation. Our multi-parameter mapping of SOS-Ras-ERK cascade activity, enabled by reconstitution of SOS1 in SOS-deficient B cells, reveals that spontaneous activation of SOS scales with SOS expression level. Essentially, the spontaneous activation of SOS is driven by Le Chatelier's principle and is simply a probabilistic event that scales with concentration. Under endogenous expression levels, this spontaneous activation must be sufficiently slow as to be inconsequential in the context of background GAP activity, thus requiring the additional boost from receptor-mediated Grb2 recruitment to trigger a productive Ras signal (see Supplementary Note 5 for an extended discussion and Supplementary Fig. 8a–d). We propose endocytosis as a method of signal attenuation, providing an actively regulated mechanism to remove SOS from the plasma membrane, effectively cutting off access to new Ras molecules. SOS constructs lacking the PR domain fail to get endocytosed and exhibit sustained ERK activation levels (further discussed in Supplementary Note 6). Thus, in its natural state, SOS activation follows a one-way trafficking circuit with active removal from the membrane via the PR domain as the shut down mechanism.

Recently, it has become clear that single amino acid variants in RasGEFs can have a profound biological effect. We established that the EF hands in RasGRP1 play a dual role in keeping this RasGEF in the autoinhibited state while simultaneously allowing for calcium-induced activation[58]. A single amino acid variant allele, *Rasgrp1*[*Anaef*], with a point-mutated EF hand perturbs both regulatory roles of this domain and leads to autoimmune features in *Rasgrp1*[*Anaef*] mice[59]. The structural basis for PR domain-facilitated autoinhibition and the transition to the activated state of SOS is unknown, since efforts to produce functional full length SOS1 protein including the PR domain have been unsuccessful to date. Mining public databases, we find several *SOS1* variants with point mutations or stop codons in the PR domain linked to Noonan developmental syndrome, hyperplastic syndromes such as hereditary gingival fibromatosis[60], and various cancers (Supplementary Fig. 8e). It is plausible that subtle point mutations in the PR domain may have significant biological effects and contribute to human disease.

online Methods

Proteins and reagents

H-Ras$^{C118S\ C181}$ (H-Ras construct containing residues 1–181 with a single cysteine at position C181 used for coupling to the bilayer, henceforth simply H-Ras), SOS^{Cat} cys-lite (residues 566–1049 with following mutations: C838A, C635A, C980S, E718C), SOS^{DPC} (residues 198–1049), SOS^{HDPC} (residues 1–1049), and SOS$^{HDPC(R552G)}$ (residues 1–1049 with R552G) of human SOS1 were expressed in *E. Coli* and purified as previously described[22]. Lipids were purchased from Avanti (Alabaster, AL). TR-DHPE, BODIPY-GDP and BODIPY-GTP were purchased from Invitrogen (Carlsbad, CA). ATTO 647N-maleimide, ATTO 488-labeled guanosine diphosphate (EDA-GDP-ATTO 488) and EDA-GppNp-ATTO 488 (non-hydrolyzeable analog of guanosine triphosphate) were purchased from Jena Bioscience (Jena, Germany). Guanosine triphosphate (GTP) was purchased from Sigma-Aldrich (Saint Louis, MO) and guanosine diphosphate (GDP) was purchased from MP biomedicals (Santa Ana, CA). Biotinylated anti-Chicken IgM was purchased from Sigma (#SAB3700240) and Cy5 labeled streptavidin was from Life Technologies (#43–4316).

Protein labeling and benchmarking

SOS constructs were fluorescently labeled by reacting 1:10 molar ratio of unlabeled protein with Atto647N-maleimide for 2 hours at 23°C. Unreacted fluorophores were removed using PD-10 columns (GE Healthcare). The degree of labeling was determined by UV Vis spectroscopy (NanoDrop 2000, Thermo Scientific) yielding; 90% for SOS^{Cat} cyslite, 119% for SOS^{DPC}, 106% for SOS^{HDPC} and 118% for SOS$^{HDPC(R552G)}$. SOS^{DPC}, SOS^{HDPC} and SOS$^{HDPC(R552G)}$ harbored multiple cysteines, explaining why labeling efficiencies exceeded 100%.

Dye labeling can potentially alter protein behavior and caution is always needed in interpretation of related results. Here, nucleotide-exchange experiments were conducted to ascertain that labeling did not alter enzyme behavior; comparison of unlabeled and labeled constructs in the stopped-flow assay indicated that labeling had negligible effect on the *in vitro* activity of SOS in our system (Supplementary Fig. 1c).

Ras-decorated supported lipid bilayers for *in vitro* assays

Ras decorated bilayers were prepared as previously described (ref.[22,38]). Lipids dissolved in chloroform were mixed in a round-bottomed flask. Solvent was evaporated by rotary evaporation (40°C, 10 min.) followed by N$_2$ flow (20 min.). Small unilamellar vesicles (SUVs) were formed by rehydrating the dried lipid film in PBS (pH 7.45). The vesicle suspension was extruded 11 times (Avestin miniextruder, 30 nm pore diameter polycarbonate membranes; Millipore, Billerica, MA). Lipid composition was 3% DOPS, 3% MCC-DOPE, 0.01% TxRed-DHPE and the balance amount of Egg-PC.

Supported lipid bilayers (SLBs) were formed by incubating the SUV suspension for 30 min. on cleaned piranha-etched glass slides mounted in flow chambers (FCS2 flow chambers, Bioptechs). The sample was then incubated with Casein in PBS (2.5 mg/ml) for 10 min.,

followed by 2.5 hours incubation with H-Ras in PBS (1 mg/ml). Following Ras incubation, unreacted MCC was quenched by treating the sample with 2-beta-mercaptoethanol in PBS (5mM) for 10 minutes. A motorized syringe pump (PHD 2000, Harvard Apparatus) was used throughout the sample preparation for liquid injections and washing steps.

For loading fluorescent nucleotide onto Ras samples were equilibrated at 4°C and washed with 3 mL loading buffer (40mM HEPES, 150mM NaCl, pH 7.4); the native nucleotide bound to Ras was stripped by 20 min. incubation with EDTA in loading buffer (50mM EDTA, 40mM HEPES, 150mM NaCl, pH7.4). This step was immediately followed by overnight incubation of samples with 10 μM fluorescent nucleotide analogue in reaction buffer (40mM HEPES, 100mM NaCl, 5mM MgCl, pH7.4). Fluorescent nucleotides used in this study included Bodipy-GDP, Bodipy-GTP, Atto488-GDP, and Atto488-GppNp. A control experiment where samples underwent all steps except Ras incubation showed no detectable non-specific binding of the applied fluorescent nucleotides to the SLB.

Immediately prior to microscopy, samples were brought to room temperature and any unbound fluorescent nucleotide was removed by washing with 3 mL reaction buffer (40mM HEPES, 100mM NaCl, 5mM $MgCl_2$, 1 mM TCEP, pH7.4) under constant flow. The two-dimensional fluidity of lipids and Ras was confirmed for each sample using fluorescence recovery after photobleaching (FRAP).

Antibody-functionalized supported lipid bilayers for live cell imaging

Bilayers for live-cell experiments were prepared as described above with a lipid composition of 5% DOPS, 0.1% Biotinyl Cap PE, 0.005% TxRed-DHPE and the balance amount of Egg-PC. A piranha-etched glass slide (#1, Fisher Scientific) mounted in a microscopy chamber (A-7816, Life Technologies) was incubated with SUV suspension (1mg/mL) for 30 min.. The sample was then treated with Cy5 labeled streptavidin (18.8 nM) for 30 min., followed by another incubation with biotinylated anti-chicken IgM (62 nM; SAB3700240, Sigma) for 30 minutes. Each incubation step was followed by copious washing with PBS.

Stopped flow supported lipid bilayer assay

Labeled and unlabeled SOS constructs were mixed at desired ratio (typically 1:20) at a total concentration of 100 nM and flowed over the bilayer as a transient pulse. The number of labeled SOS molecules remaining on the bilayer after the pulse (due to capture by catalytic Ras in the absence of free nucleotide[30,40] was counted at the single molecule level and used to infer the recruitment probability (see Supplementary Note 7). It was confirmed experimentally that SOS in our system indeed was stably tethered to the bilayer via Ras in the absence of free nucleotide. For Y64A experiments SOS engaged the membrane in a transient manner (Fig. 2c) and the extent of binding was inferred from the observed peak binding during the SOS pulse instead of from the plateau (see data in Fig. 2d).

The nucleotide exchange reaction was initiated by providing a continuous flow of nucleotide (120 μM GDP or GTP). SOS desorption and nucleotide exchange kinetics were quantified at different time-points by acquiring an image of the fluorescent nucleotide on Ras and 10 images of the labeled SOS. For each time-point we imaged at a different position in the flow chamber to avoid bleaching. The 10 images of SOS for each position allowed us to discard

immobile SOS in the analysis (i.e., SOS bound to defects in the bilayer). This is a crucial aspect of the experimental design as it avoids bias from sample-to-sample variation in the number of defects as well as possible differential tendencies of various protein constructs to adhere to bilayer defects. By counting membrane-bound SOS based on single molecule tracking we can focus entirely on species that are laterally mobile.

A clear demonstration that the assay probes specific interactions between Ras and SOS comes from the observation that all SOS constructs tested exhibit sensitivity to the nucleotide state of Ras with consistently increased recruitment probability as well as prolonged residency period on membranes displaying RasGTP (Fig. 2d, Supplementary Fig. 3a–c).

For specific comparison of desorption for successfully activated SOS constructs (Fig. 3c) traces were normalized to the SOS count at the membrane observed at the initiation of the nucleotide chase. For SOS[Cat] we observed a fraction of rapidly desorbing species during the first few seconds of the chase (Fig. 2c). This fast desorbing fraction was not contributing to processive Ras turnover (Supplementary Fig. 1d) and for the comparison with other constructs in Figure 3c and Supplementary Figure 3b,c we cropped the first 10 s of the trace.

Maintenance and transfection of DT40 and Jurkat cell lines

Culture maintenance, plasmid transfection and BCR stimulation of chicken DT40 B cell lines were carried out as previously described[46]. Jurkat cell culture and transfection techniques were also performed as described[8]. The SOS1⁻2⁻deficient DT40 B cells were generated in Dr. Tomohiro Kurosaki's laboratory (RIKEN). Both wildtype and SOS1⁻2⁻ deficient DT40 B cells were gifts from Dr. Kurosaki. Obtained cell lines were confirmed to be free of mycoplasma contamination. For routine cell functional authentication, surface expression of B cell receptor (BCR) was confirmed by flow cytometry and by BCR-induced pERK2 measurement similar to the experiment shown in Supplementary Figure 4. Jurkat T cells were obtained from ACCC and were maintained according to the provided guideline.

To generate EGFP-tagged hSOS1 variants, EGFP coding sequence (CDS) was PCR-amplified with Xba I- and Not I-flanked primers from pEGFP-N1 plasmid (Clonetech). Resulting SOS1-EGFP construct bears a 5 amino acid linker (SRGGR) between SOS1 and EGFP CDS. Expression was confirmed by Western blotting with anti-GFP antibody (Supplementary Fig. 4a).

Live cell imaging

For live cell microscopy, 2.5 million cells were exchanged from cell culture media to 1mL of serum-free RPMI by pelleting cells with 5 min. centrifugation at 500 g, followed by 30 min. incubation in serum-free RPMI at 37°C. Cells were imaged in pH 7.40, 10 mM HEPES, 68 mM NaCl, 2.5 mM KCl, 0.35 mM Na_2HPO4, 3 mM D-Glucose, 1 mM $CaCl_2$, 2 mM $MgCl_2$, 0.1% BSA.

Live-cell imaging was performed using a stage-top incubator and an objective heater (Chamlide TC-A, Quorum Technology, Guelph, Canada). Experiments were initiated by adding cells to SLBs functionalized with an antibody for the BCR. The bilayer was heated to

37°C prior to addition of cells. 488nm channel (SOS-EGFP) and 640nm channel (BCR engaged antibody on SLBs) For a few selected cells TIRF images were acquired every ~1–5 minutes to follow the kinetics of the signaling reaction. After ~30 min. of adding cells to the chamber, 488nm and 640nm TIRF, together with bright field and RICM micrographs were acquired at a number of positions in the microscope chamber.

Flow cytometry and data analysis

Jurkat T cells were transiently transfected for 20 hours with 10 μg of wild-type or allosteric mutant (W729E) SOS^{Cat}-encoding plasmid together with 10 μg of GFP plasmid. The activity of Ras-ERK pathway was measured by FACS staining of surface CD69 (sCD69, BD; #555531) together with GFP intensity measurement. GFP-positive cells were sub-gated into 9 fractions. Geometric mean fluorescence of CD69 level was determined for each fraction.

For quantitative and qualitative assay of RAS-ERK signal module, intracellular staining of BCR-induced ERK phosphorylation was performed according to established procedures[46]. In brief, cells were stimulated with BCR crosslinking mouse IgM (clone M4) for desired time period. Stimulation was then stopped by adding 4% paraformaldehyde-PBS, and cells were fixed for 20 min at room temperature. Fixed cells were washed three times with FACS wash buffer (PBS;1% BSA;10mM EDTA) and subsequently permeabilized with pre-chilled 90% methanol overnight. Cells were then washed three times with FACS wash buffer and stained for pERK with rabbit anti-sera (Cell signaling #9101). pERK was visualized by secondary staining with goat anti-rabbit IgG conjugated with APC (Jackson immunochemicals; #711-136-152).

For FACS acquisition, a minimum of 100,000 events were collected for each time point using FACS Calibur machine (BD) and analyzed by FlowJo software. For analysis of ERK activation, cells were sorted in nine bins of equal interval according to their SOS expression level. Subsets with less than 100 acquired events were disregarded for fair comparison of SOS1 variants with different expression level.

COS1 cell transfections and immunofluorescence staining

COS1 cells were cultured and treated as previously described[22]. COS1 cells were obtained from ACCC. In brief, cells grown on cover slips were transfected with either the pCGT-T7-SOS^{Cat} or SOS$^{Cat-L687E, R688A}$) constructs together with GFP-tagged H-Ras$^{A59G, D38E_}$-encoding plasmid. After 24 h, transfected cells were fixed in 3.7% (v/v) formaldehyde and permeabilized with 0.1% (v/v) Triton X-100. Expressed SOS proteins were visualized by staining with anti-T7 antibody (EMD Millipore; #AB3790), followed by rhodamine-conjugated anti-mouse antibody (Cappel; #R-6393). Rab5 protein was expressed as a GFP fusion protein. EGF was obtained from Invitrogen. Imaging was conducted on a Zeiss Axiovert 200M microscope.

Optical microscopy platforms

Epi-fluorescence and total internal reflection fluorescence (TIRF) microscopy was performed on a Nikon Eclipse Ti inverted microscope with a Nikon Apo TIRF 100× oil

immersion objective (1.49 NA) and an EMCCD camera (Andor iXon 597DU, Andor Inc., South Windsor, CT). A mercury arc lamp was used for epi-fluorescence illumination. 488 nm (Sapphire HP; Coherent Inc., Santa Clara, CA) and 647 nm (RCL-050-640; Crystalaser, Reno, NV) lasers were used for through the objective TIRF imaging. Bandpass emission filters for 488 and 647 nm TIRF images were HQ515/30 and HQ700/75 (Chroma Technology Corp., Bellows Falls, VT), respectively. The microscope was operated using MetaMorph software (Molecular Devices Corp., Downington, PA).

For live cell experiments, an additional TIRF setup was employed with the following specifications: Inverted microscope body (Nikon Eclipse Ti (Ti HUBC/A), Technical Instruments, Burlingame, CA) equipped with a Nikon Apo TIRF 100× oil objective (1.49 NA). The microscope had a custom-built laser launch with 488 nm, 561 nm and 633 nm lasers (all from the OBIS product line, Coherent Inc. Santa Clara, CA) controlled via a laser control module (OBIS scientific remote). The TIRF setup operated in through the objective mode and images were collected on an EMCCD (iXon ultra 897, Andor Inc., South Windsor, CT). The microscope was controlled using μManager[61].

Confocal microscopy was performed on a custom build spinning disk confocal system[62]. Briefly, images were captured using a Nikon Apo TIRF 100× oil immersion objective (1.49 NA) and an EMCCD (Andor iXon3 888, Belfast, Ireland) and the microscope was controlled using μManager[61]. Axial slice step size was 0.5 μm.

Data analysis

A detailed description of data analysis procedures relating to imaging experiments can be found in Supplementary Note 7.

Supplementary Material

Refer to Web version on PubMed Central for supplementary material.

Acknowledgments

References

1. Campbell SL, Khosravi-Far R, Rossman KL, Clark GJ, Der CJ. Increasing complexity of Ras signaling. Oncogene. 1998; 17:1395–1413. [PubMed: 9779987]

2. Chang L, Karin M. Mammalian MAP kinase signalling cascades. Nature. 2001; 410:37–40. [PubMed: 11242034]

3. Karnoub AE, Weinberg RA. Ras oncogenes: split personalities. Nat. Rev. Mol. Cell Biol. 2008; 9:517–531. [PubMed: 18568040]

4. Stephen AG, Esposito D, Bagni RK, McCormick F. Dragging ras back in the ring. Cancer Cell. 2014; 25:272–281. [PubMed: 24651010]

5. McCormick F. Signal transduction. How receptors turn Ras on. Nature. 1993; 363:15–16. [PubMed: 8479530]

6. Findlay GM, Pawson T. How is SOS activated? Let us count the ways. Nat. Struct. Mol. Biol. 2008; 15:538–540. [PubMed: 18523461]

7. Groves JT, Kuriyan J. Molecular mechanisms in signal transduction at the membrane. Nat. Struct. Mol. Biol. 2010; 17:659–665. [PubMed: 20495561]

8. Das J, et al. Digital signaling and hysteresis characterize ras activation in lymphoid cells. Cell. 2009; 136:337–351. [PubMed: 19167334]

9. Jun JE, Rubio I, Roose JP. Regulation of Ras exchange factors and cellular localization of Ras activation by lipid messengers in T cells. Frontiers Immunol. 2013; 4

10. Egan SE, et al. Association of Sos Ras exchange protein with Grb2 is implicated in tyrosine kinase signal transduction and transformation. Nature. 1993; 363:45–51. [PubMed: 8479536]

11. Genot E, Cantrell DA. Ras regulation and function in lymphocytes. Curr. Opin. Immunol. 2000; 12:289–294. [PubMed: 10781411]

12. Kortum RL, et al. Targeted Sos1 deletion reveals its critical role in early T-cell development. Proc. Natl. Acad. Sci. U.S.A. 2011; 108:12407–12412. [PubMed: 21746917]

13. Baltanas FC, et al. Functional redundancy of Sos1 and Sos2 for lymphopoiesis and organismal homeostasis and survival. Mol. Cell Biol. 2013; 33:4562–4578. [PubMed: 24043312]

14. Wang DZ, et al. Mutation in Sos1 dominantly enhances a weak allele of the EGFR, demonstrating a requirement for Sos1 in EGFR signaling and development. Genes Dev. 1997; 11:309–320. [PubMed: 9030684]

15. Findlay GM, et al. Interaction domains of sos1/grb2 are finely tuned for cooperative control of embryonic stem cell fate. Cell. 2013; 152:1008–1020. [PubMed: 23452850]

16. Buday L, Downward J. Epidermal growth factor regulates p21ras through the formation of a complex of receptor, Grb2 adapter protein, and Sos nucleotide exchange factor. Cell. 1993; 73:611–620. [PubMed: 8490966]

17. Gale NW, Kaplan S, Lowenstein EJ, Schlessinger J, Bar-Sagi D. Grb2 mediates the EGF-dependent activation of guanine nucleotide exchange on Ras. Nature. 1993; 363:88–92. [PubMed: 8386805]

18. Li N, et al. Guanine-nucleotide-releasing factor hSos1 binds to Grb2 and links receptor tyrosine kinases to Ras signalling. Nature. 1993; 363:85–88. [PubMed: 8479541]

19. Rozakis-Adcock M, Fernley R, Wade J, Pawson T, Bowtell D. The SH2 and SH3 domains of mammalian Grb2 couple the EGF receptor to the Ras activator mSos1. Nature. 1993; 363:83–85. [PubMed: 8479540]

20. Waterman H, et al. A mutant EGF-receptor defective in ubiquitylation and endocytosis unveils a role for Grb2 in negative signaling. EMBO J. 2002; 21:303–313. [PubMed: 11823423]

21. Chardin P, et al. Human Sos1: a guanine nucleotide exchange factor for Ras that binds to GRB2. Science. 1993; 260:1338–1343. [PubMed: 8493579]

22. Gureasko J, et al. Membrane-dependent signal integration by the Ras activator Son of sevenless. Nat. Struct. Mol. Biol. 2008; 15:452–461. [PubMed: 18454158]

23. Gureasko J, et al. Role of the histone domain in the autoinhibition and activation of the Ras activator Son of Sevenless. Proc. Natl. Acad. Sci. U.S.A. 2010; 107:3430–3435. [PubMed: 20133692]

24. Yadav KK, Bar-Sagi D. Allosteric gating of Son of sevenless activity by the histone domain. Proc. Natl. Acad. Sci. U.S.A. 2010; 107:3436–3440. [PubMed: 20133694]

25. Margarit SM, et al. Structural evidence for feedback activation by Ras.GTP of the Ras-specific nucleotide exchange factor SOS. Cell. 2003; 112:685–695. [PubMed: 12628188]

26. Roberts AE, et al. Germline gain-of-function mutations in SOS1 cause Noonan syndrome. Nat. Genet. 2007; 39:70–74. [PubMed: 17143285]

27. Tumurkhuu M, Saitoh M, Takita J, Mizuno Y, Mizuguchi M. A novel SOS1 mutation in Costello/CFC syndrome affects signaling in both RAS and PI3K pathways. J Recept. Signal. Transduct. Res. 2013; 33:124–128. [PubMed: 23528009]

28. Kholodenko BN, Hoek JB, Westerhoff HV. Why cytoplasmic signalling proteins should be recruited to cell membranes. Trends Cell Biol. 2000; 10:173–178. [PubMed: 10754559]

29. Karlovich CA, et al. In vivo functional analysis of the Ras exchange factor son of sevenless. Science. 1995; 268:576–579. [PubMed: 7725106]

30. Corbalan-Garcia S, Margarit SM, Galron D, Yang SS, Bar-Sagi D. Regulation of Sos activity by intramolecular interactions. Mol. Cell Biol. 1998; 18:880–886. [PubMed: 9447984]

31. McCollam L, et al. Functional roles for the pleckstrin and Dbl homology regions in the Ras exchange factor Son-of-sevenless. J. Biol. Chem. 1995; 270:15954–15957. [PubMed: 7608150]

32. Wang W, et al. The Grb2 binding domain of mSos1 is not required for downstream signal transduction. Nat. Genet. 1995; 10:294–300. [PubMed: 7670467]

33. Zhao C, Du G, Skowronek K, Frohman MA, Bar-Sagi D. Phospholipase D2-generated phosphatidic acid couples EGFR stimulation to Ras activation by Sos. Nat. Cell Biol. 2007; 9:706–712. [PubMed: 17486115]

34. Roose JP, Mollenauer M, Ho M, Kurosaki T, Weiss A. Unusual interplay of two types of Ras activators, RasGRP and SOS, establishes sensitive and robust Ras activation in lymphocytes. Mol. Cell. Biol. 2007; 27:2732–2745. [PubMed: 17283063]

35. Chen RH, Corbalan-Garcia S, Bar-Sagi D. The role of the PH domain in the signal-dependent membrane targeting of Sos. EMBO J. 1997; 16:1351–1359. [PubMed: 9135150]

36. Groves JT, Ulman N, Boxer SG. Micropatterning fluid lipid bilayers on solid supports. Science. 1997; 275:651–653. [PubMed: 9005848]

37. Groves JT, Boxer SG. Micropattern formation in supported lipid membranes. Acc. Chem. Res. 2002; 35:149–157. [PubMed: 11900518]

38. Iversen L, et al. Ras activation by SOS: allosteric regulation by altered fluctuation dynamics. Science. 2014; 345:50–54. [PubMed: 24994643]

39. Lin WC, et al. H-Ras forms dimers on membrane surfaces via a protein-protein interface. Proc. Natl. Acad. Sci. U.S.A. 2014; 111:2996–3001. [PubMed: 24516166]

40. Bos JL, Rehmann H, Wittinghofer A. GEFs and GAPs: critical elements in the control of small G proteins. Cell. 2007; 129:865–877. [PubMed: 17540168]

41. Boykevisch S, et al. Regulation of ras signaling dynamics by Sos-mediated positive feedback. Curr. Biol. 2006; 16:2173–2179. [PubMed: 17084704]

42. Hall BE, Yang SS, Boriack-Sjodin PA, Kuriyan J, Bar-Sagi D. Structure-based mutagenesis reveals distinct functions for Ras switch 1 and switch 2 in Sos-catalyzed guanine nucleotide exchange. J. Biol. Chem. 2001; 276:27629–27637. [PubMed: 11333268]

43. Sondermann H, et al. Structural analysis of autoinhibition in the Ras activator Son of sevenless. Cell. 2004; 119:393–405. [PubMed: 15507210]

44. Kubiseski TJ, Chook YM, Parris WE, Rozakis-Adcock M, Pawson T. High affinity binding of the pleckstrin homology domain of mSos1 to phosphatidylinositol (4,5)-bisphosphate. J. Biol. Chem. 1997; 272:1799–1804. [PubMed: 8999863]

45. Oh-hora M, Johmura S, Hashimoto A, Hikida M, Kurosaki T. Requirement for Ras guanine nucleotide releasing protein 3 in coupling phospholipase C-gamma2 to Ras in B cell receptor signaling. J. Exp. Med. 2003; 198:1841–1851. [PubMed: 14676298]

46. Jun JE, Li M, Chen H, Chakraborty AK, Roose JP. Activation of ERK but not of p38 MAP kinase Pathways in Lymphocytes Requires Allosteric Activation of SOS. Mol. Cell Biol. 2013; 33:2470–2484. [PubMed: 23589333]

47. Sondermann H, Nagar B, Bar-Sagi D, Kuriyan J. Computational docking and solution x-ray scattering predict a membrane-interacting role for the histone domain of the Ras activator son of sevenless. Proc. Natl. Acad. Sci. U.S.A. 2005; 102:16632–16637. [PubMed: 16267129]

48. Aronheim A, et al. Membrane targeting of the nucleotide exchange factor Sos is sufficient for activating the Ras signaling pathway. Cell. 1994; 78:949–961. [PubMed: 7923364]

49. Mossman KD, Campi G, Groves JT, Dustin ML. Altered TCR signaling from geometrically repatterned immunological synapses. Science. 2005; 310:1191–1193. [PubMed: 16293763]

50. Davey AM, Liu W, Sohn HW, Brzostowski J, Pierce SK. Understanding the initiation of B cell signaling through live cell imaging. Meth. Enzymol. 2012; 506:265–290. [PubMed: 22341229]

51. Balagopalan L, Sherman E, Barr VA, Samelson LE. Imaging techniques for assaying lymphocyte activation in action. Nat. Rev. Immunol. 2011; 11:21–33. [PubMed: 21179118]

52. Grakoui A, et al. The Immunological Synapse: A Molecular Machine Controlling T Cell Activation. Science. 1999; 285:221–227. [PubMed: 10398592]

53. Weber M, et al. Phospholipase C-gamma2 and Vav cooperate within signaling microclusters to propagate B cell spreading in response to membrane-bound antigen. J Exp Med. 2008; 205:853–868. [PubMed: 18362175]

54. Brdicka T, et al. Non-T cell activation linker (NTAL): A transmembrane adaptor protein involved in immunoreceptor signaling. J. Exp. Med. 2002; 196:1617–1626. [PubMed: 12486104]

55. Janssen E, Zhu MH, Zhang WJ, Koonpaew S, Zhang WG. LAB: A new membrane-associated adaptor molecule in B cell activation. Nat. Immunol. 2003; 4:117–123. [PubMed: 12514734]

56. Pierce SK, Liu W. The tipping points in the initiation of B cell signalling: how small changes make big differences. Nat. Rev. Immunol. 2010; 10:767–777. [PubMed: 20935671]

57. Stenmark H. Rab GTPases as coordinators of vesicle traffic. Nat. Rev. Mol. Cell Biol. 2009; 10:513–525. [PubMed: 19603039]

58. Iwig JS, et al. Structural analysis of autoinhibition in the Ras-specific exchange factor RasGRP1. eLife. 2013; 2:e00813. [PubMed: 23908768]

59. Daley SR, et al. Rasgrp1 mutation increases naïve T-cell CD44 expression and drives mTOR-dependent accumulation of Helios+ T cells and autoantibodies. eLife. 2013; 2:e01020. [PubMed: 24336796]

60. Rojas JM, Oliva JL, Santos E. Mammalian Son of Sevenless Guanine Nucleotide Exchange Factors: Old Concepts and New Perspectives. Genes & Cancer. 2011; 2:298–305. [PubMed: 21779500]

online Methods references

61. Edelstein A, Amodaj N, Hoover K, Vale R, Stuurman N. Computer control of microscopes using microManager. Curr. Protoc. Mol. Biol. 2010; Chapter 14(Unit 14):20. [PubMed: 20890901]

62. Greene AC, et al. Spatial organization of EphA2 at the cell-cell interface modulates trans-endocytosis of ephrinA1. Biophys. J. 2014; 106:2196–2205. [PubMed: 24853748]
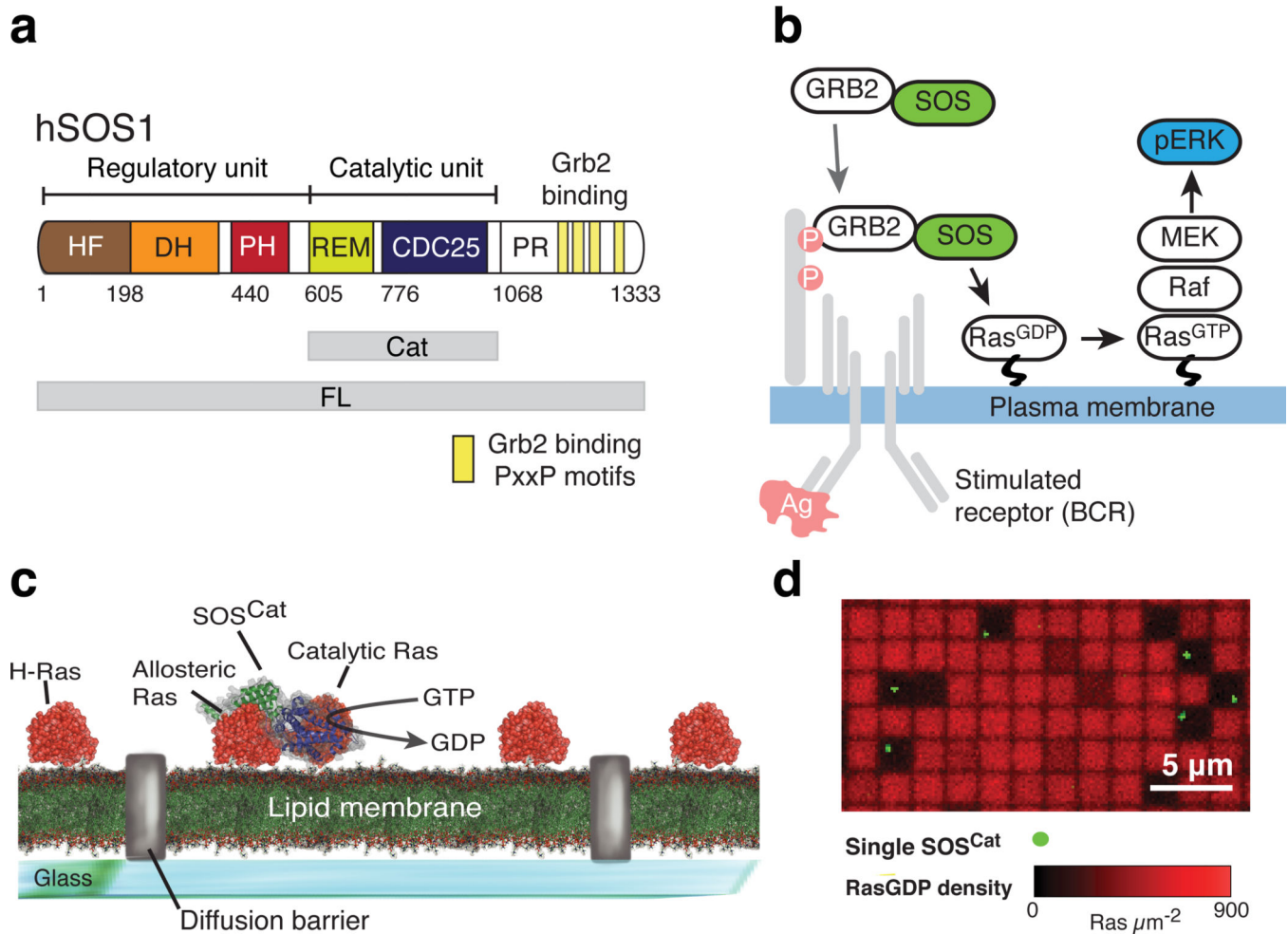
Figure 1. The catalytic core of SOS is stably and functionally recruited to Ras-decorated supported lipid bilayers *in vitro*, independently of Grb2 and lipid binding domains

(**a**) The domain architecture of full-length (FL) human SOS1 (hSOS1). The catalytic unit (Cat) is depicted together with the flanking regulatory domains. Yellow boxes in the C-terminal proline rich (PR) domain indicate PxxP motifs known to interact with Grb2.

(**b**) Classical model of SOS-Ras-ERK signal transduction pathway. In the shown example, SOS is recruited to the plasma membrane downstream of activated B cell receptor via binding of Grb2 to phosphotyrosine motifs on the adaptor protein LAB.

(**c**) Single SOS activity assay based on micro-patterned Ras functionalized fluid supported lipid bilayers.

(**d**) Representative overlay image of fluorescent GDP bound to Ras (red channel) and membrane-recruited SOS^{Cat} (green channel) in the single molecule assay depicted in **c**. Membrane corrals where individual copies of SOS^{Cat} were recruited have depleted signal and appear darker in the GDP channel, demonstrating highly processive SOS^{Cat} activity (i.e., recruited SOS activates Ras in a sustained manner without dissociating from the membrane surface). The particular experiment was repeated five times.
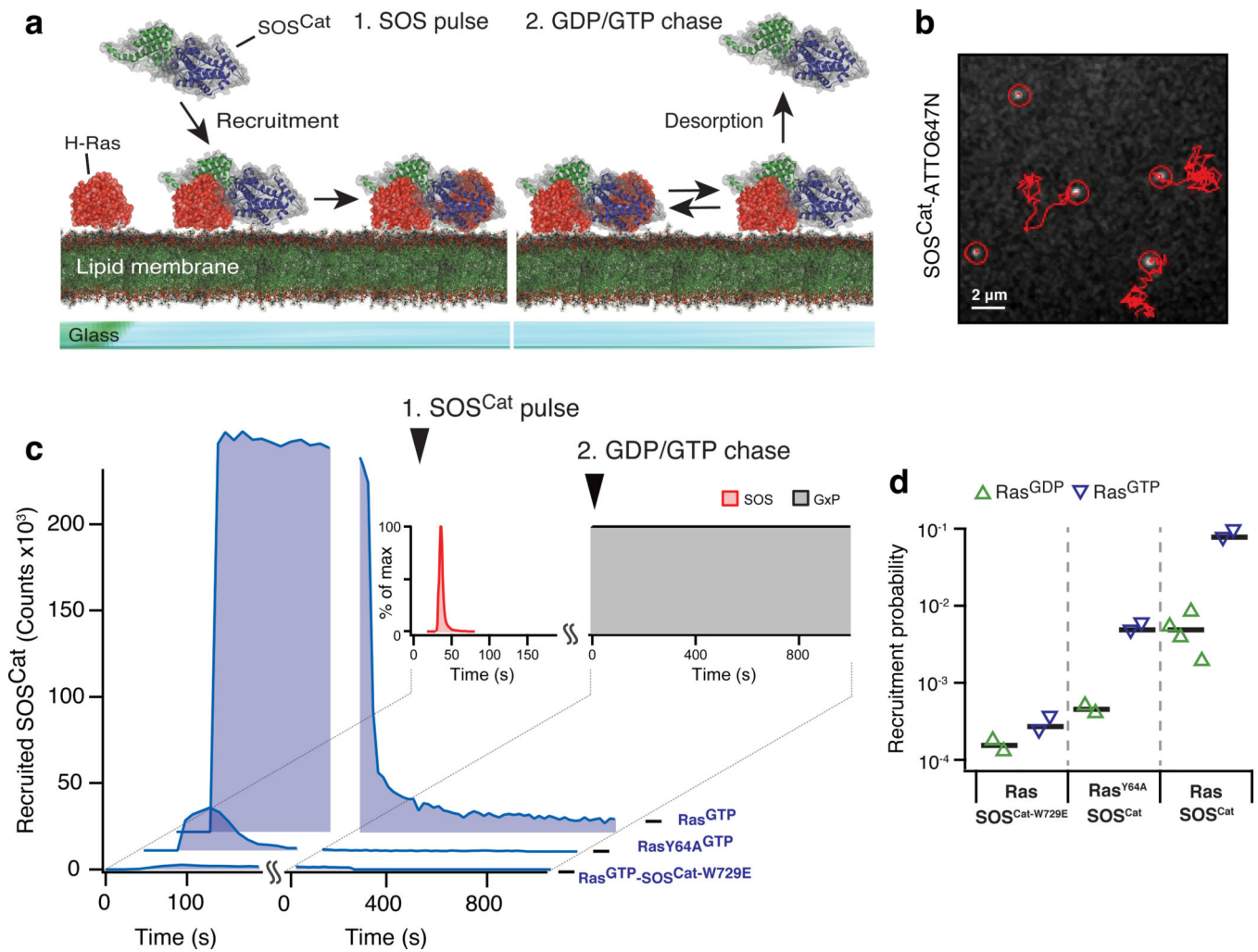
Figure 2. Stopped flow supported lipid bilayer assay probing SOS recruitment and desorption

(**a**) Cartoon representation of the two phases of the assay.

(**b**) Single molecule tracking of ATTO647N labeled SOS^{Cat} diffusing at the bilayer.

(**c**) Traces from the stopped flow assay. In addition to SOS^{Cat} the panel shows experiments with SOS$^{Cat-W729E}$, a mutant with an abolished allosteric pocket, and Ras^{Y64A}, a construct deficient in binding to the active site of SOS. The indicated counts are for a field of view of 55×55 µm^2 and were scaled by taking into account the applied ratio of unlabeled to labeled enzymes.

(**d**) Membrane recruitment probabilities quantified from phase 1 of the stopped flow assay. Each triangle represents data from a SLB sample. Black horizontal lines indicate the average of the data shown for each condition.

Source data for plots and graphs are available online.
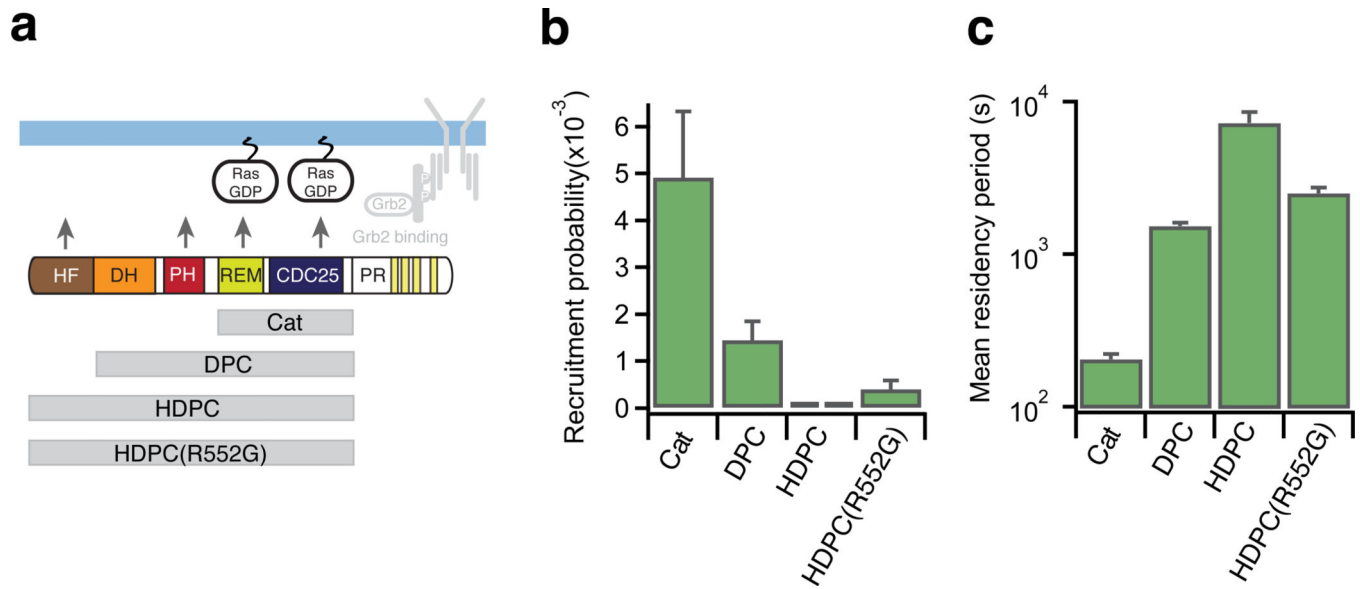
Figure 3. N-terminus of SOS is suppressing bilayer recruitment while prolonging dwell time in the active membrane bound state

(**a**) SOS constructs tested in the stopped flow supported bilayer assay. All experiments shown were conducted with RasGDP on the bilayer.

(**b**) Recruitment probability of SOS constructs obtained from the stopped flow assay. Each bar represents the average of data collected at N SLB samples, except for HDPC where each bar reflects data from one SLB: SOS^{Cat} N=4, DPC N=4, HDPC N=2, HDPC(R552G) N=3. Each sample was imaged at least at 15 different positions. Error bars represent SEM. (data for SOS^{Cat} are re-plotted from Figure 2 for comparison).

(**c**) Membrane residence time of SOS constructs obtained from the stopped flow assay. The mean residency period for each construct was obtained by fitting desorption traces (Supplementary Fig. 3b, N SLB samples: SOS^{Cat} N=5, DPC N=4, HDPC N=2, HDPC(R552G) N=3). Error bars indicate estimated standard deviation on the fit coefficient for an average over the indicated samples.

Source data for plots and graphs are available online.
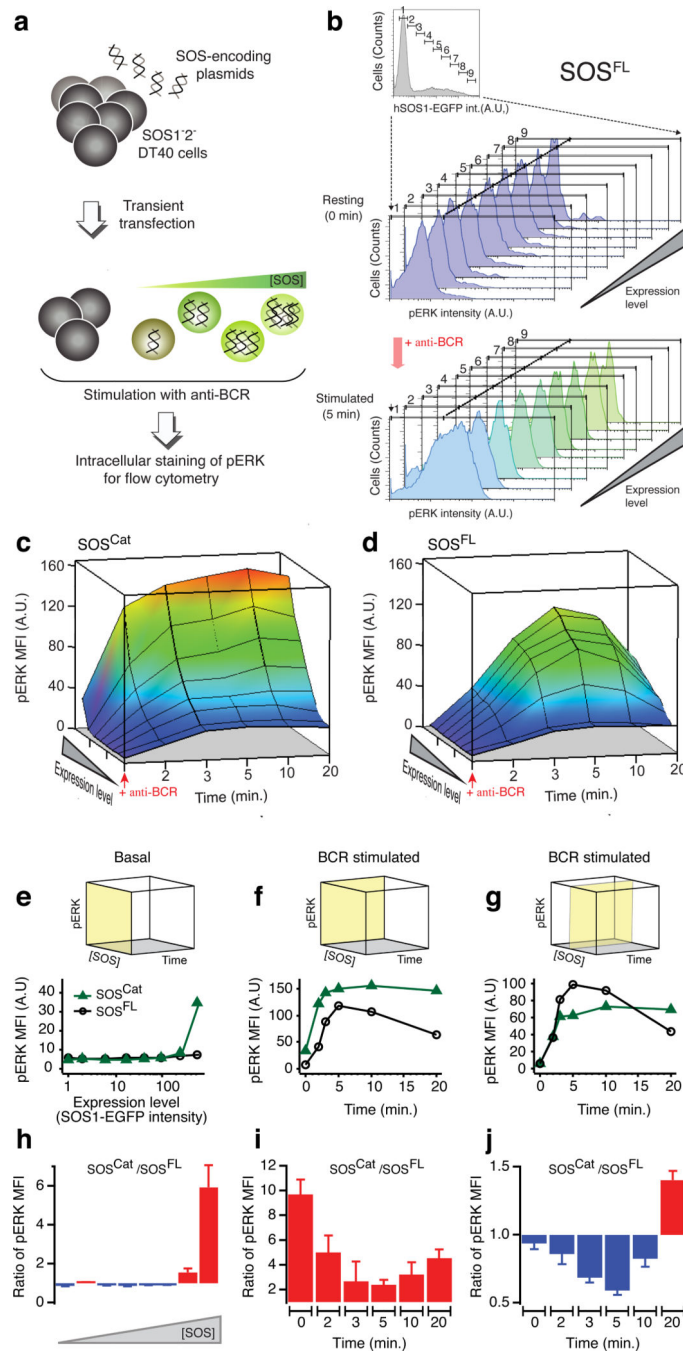
Figure 4. Multi-parameter assay of SOS-RAS-ERK pathway activity reveals functional significance of SOS flanking domains in cell signaling context

(**a**) p-FLOW assay of phospho-ERK (pERK) in transiently transfected SOS1$^-$2$^-$ DT40 B cells.

(**b**) Multi-parameter analysis of SOS-RAS-ERK pathway in model B cells expressing full-length hSOS1 (SOS^{FL}) C-terminally fused to an EGFP label.

(**c–d**) BCR-induced SOS-RAS-ERK pathway activation as a function of increasing SOS expression level and time after stimulation of BCR for SOS^{Cat}- and SOS^{FL}-expressing cells.

Arrow heads indicate the time of BCR activation. pERK level is reported as mean fluorescence intensity (MFI).

(**e**) Comparison of basal pERK level across increasing protein concentration of SOS^{Cat} and SOS^{FL}. The yellow plane on the cube indicates the subspace of the 3D parameter space of the assay corresponding to the shown traces.

(**f–g**) Comparative plots representing the dynamic change in BCR-induced pERK as a function of stimulation time in cells expressing super-physiological level (f) and intermediate level of SOS (g).

(**h–j**) Ratio's of pERK observed in SOS^{Cat}- and SOS^{FL}-transfected cells corresponding to traces on panels e–g. Red fill indicates increased activity of SOS^{Cat} as compared to SOS^{FL} whereas blue fill highlights decreased relative activity. Data are based on seven independent cell cultures and p-FLOW experiments. Error bars represent SEM.

Source data for plots and graphs are available online.
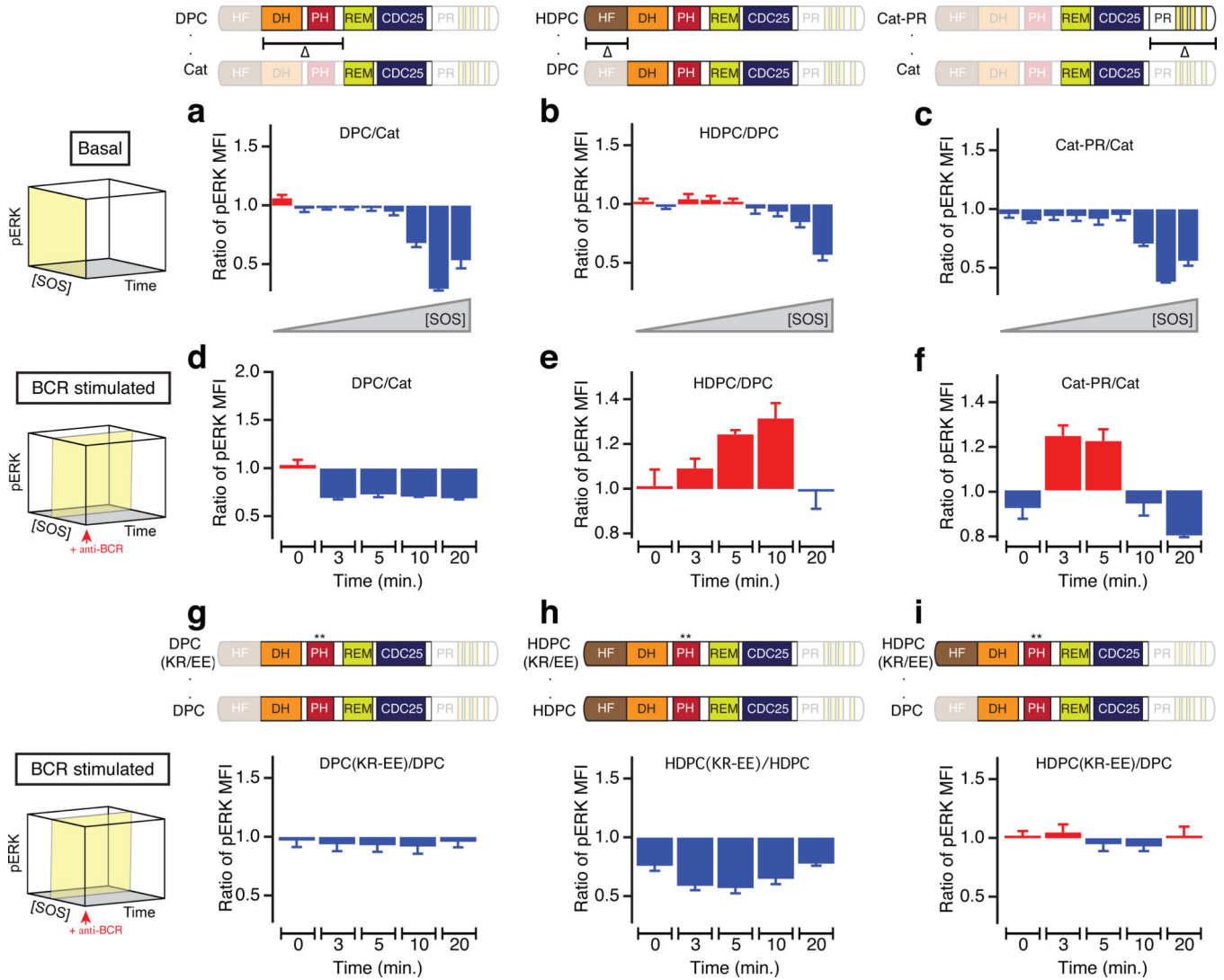
Figure 5. SOS^{Cat} flanking domains block spontaneous activation in basal state but promote RAS-ERK signal transduction following receptor stimulation

(**a,b,c**) Addition of SOS^{Cat}-flanking domains inhibits spontaneous activation of ERK in the p-FLOW assay: DH-PH domain (**a**), HF domain (**b**) and PR domain (**c**) (depicted schematically in domain diagrams at the top). The ratio of pERK MFI for longer to shorter SOS variants is plotted against increasing SOS concentration for unstimulated cells (basal state).

(**d,e,f**) Time dependence of pERK MFI ratio after BCR stimulation is plotted for indicated constructs: DH-PH domain (**d**), HF domain (**e**), and PR domain (**f**) (depicted schematically in domain diagrams at the top).

(**g,h,i**) BCR-induced ERK activation is compared between KR-EE PH domain mutant against indicated wild-type SOS1 variants. The K456E R459E (KR-EE, **) mutation disrupts membrane lipid interaction mediated by PH domain.
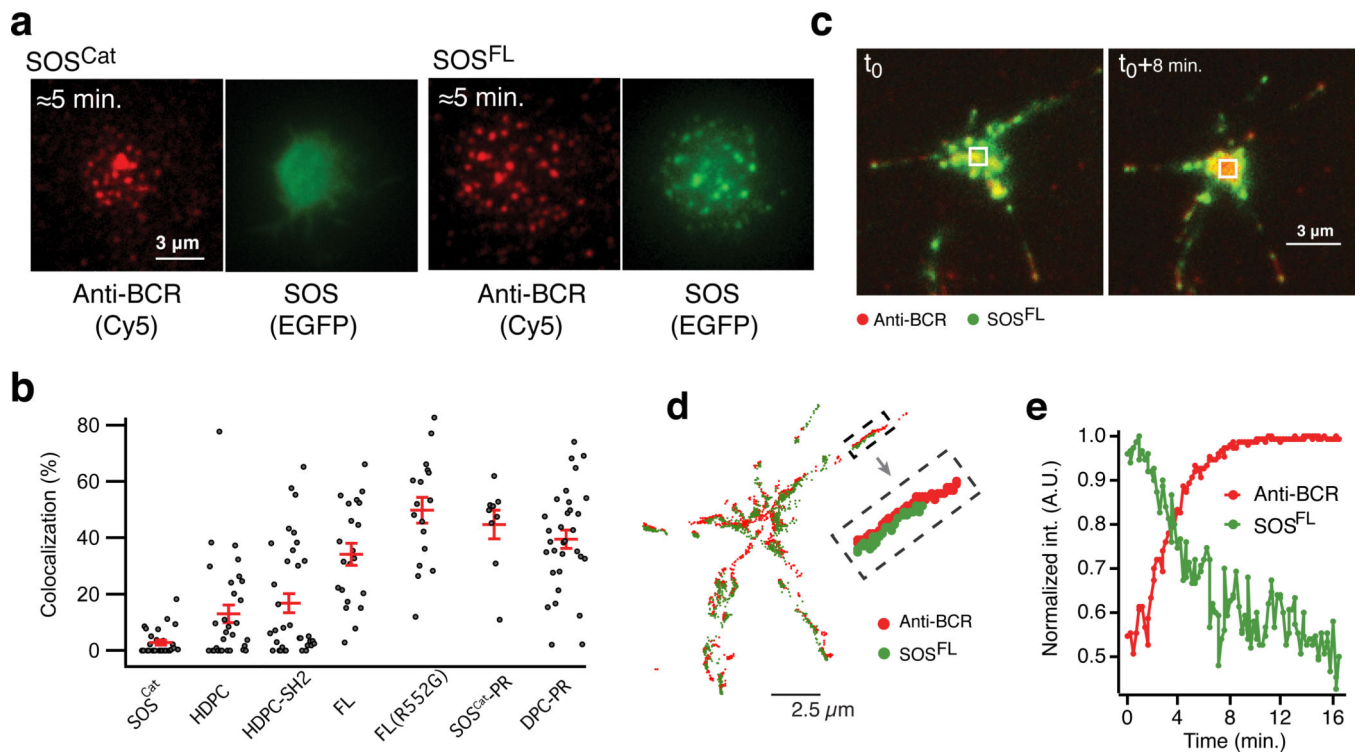
Yellow planes on the cubes to the left indicate the corresponding subspace of the 3D parameter space in the p-FLOW assay (c.f., Fig. 4c,d). Data are based on three independent experiments. Error bars represent SEM.

Source data for plots and graphs are available online.

Figure 6. PR domain dependent localization of SOS to BCR microclusters and SOS depletion from the central BCR cluster formed between B cells and supported lipid bilayers decorated with BCR crosslinking antibody

(**a**) Representative TIRFM images illustrating spatial localization of SOS^{FL} and BCR microclusters. The panel shows, respectively, **a** cell expressing SOS^{Cat} (left) and SOS^{FL} (right) at early (≈5 min.) time point after contacting the bilayer. See (b) for number of replications.

(**b**) Colocalization of different SOS variants and BCR microclusters. Each dot on the graph represents data from one cell. Red horizontal lines indicate average ± SEM for the shown scatter data. N cells;N SLB samples: SOS^{Cat} 31;5, HDPC 29;2, HDPC-SH2 34;2, 29;2 FL 21;2, FL(R552G) 16;2, SOSCat-PR 9;2, DPC-PR 32;1.

(**c**) Overlay of anti-BCR (cy5, red) and SOS (EGFP, green) fluorescence signal before (left) and after (right) the formation of a central BCR cluster. The displayed overlays are also plotted as separate image channels in Supplementary Figure 7c.

(**d**) Trajectories of BCR (red) and SOS^{FL} (green) movement at the cell-bilayer interface. The trajectories were obtained by tracking individual BCR and SOS clusters in a time-lapse (Movie S1) of the cell shown in (c). Each tracked position of a microcluster is indicated by a dot. Chains of connected dots draw out microcluster trajectories.

(**e**) Normalized time-traces of the fluorescence intensity of SOS^{FL}-EGFP and BCR at the center of the cell-supported bilayer synapse for the cell shown in **c**. The phenomenon of SOS depletion from the central BCR cluster was observed for 69% of SOS^{FL} expressing cells (95 cells imaged over 5 experiments).

Source data for plots and graphs are available online.
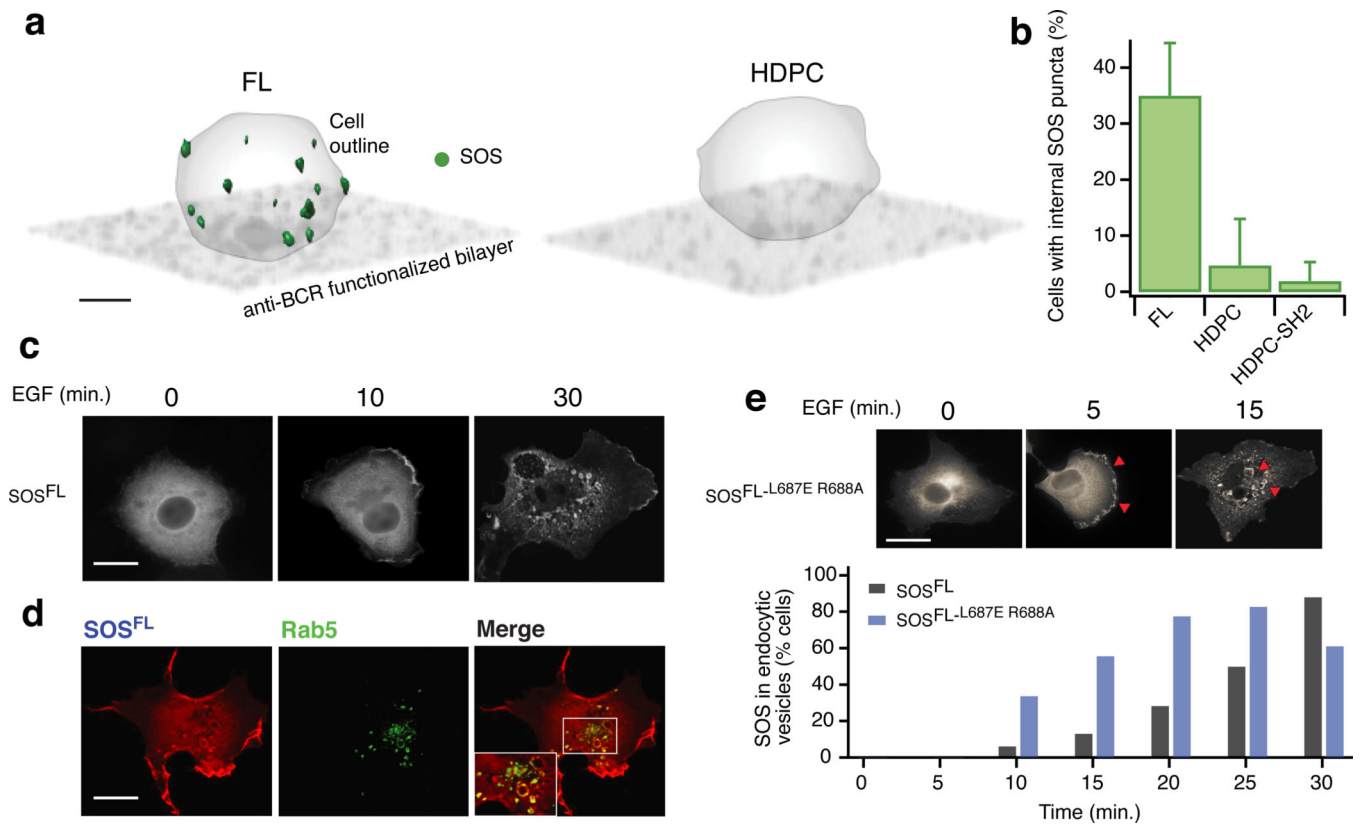
Figure 7. PR domain dependent SOS endocytosis mediates signal attenuation

(**a**) Confocal data in 3D rendering showing SOS^{FL} enriched vesicle-like structures appearing away from the cell-bilayer contact zone at late time points (≈10–30 min. after cell landing). Bar: 3 μm.

(**b**) Statistics of cells displaying internal SOS puncta as shown in **a**. N cells;N SLB samples;N cell cultures: FL 97;4;2, HDPC 75;3;2, HDPC-SH2 78;3;2. Error bars indicate SD over the different SLB samples.

(**c**) Localization of EGFP-tagged full length SOS1 in COS-1 cells stimulated with EGF for the indicated time points. Bar: 10 μm.

(**d**) Colocalzation of internalized SOS1 with the Rab5 endosomal marker in COS-1 cells stimulated for 25 minutes with EGF. Images shown are representative of colocalization pattern observed in >75% of the cells in 3 independent experiments (25 cells analyzed per experiment). The enlarged inset in the merge is also plotted in Supplementary Figure 7d as separate image channels. Bar: 10 μm.

(**e**) Kinetics of SOS localization to endocytic vesicles in EGF stimulated COS-1 cells. EGFP-tagged SOS^{FL} is compared to a full length SOS1 molecule with a functionally impaired allosteric pocket (SOS$^{FL-L687E, R688A}$). Representative images accompany the bar graph. The results represent an average of two independent experiments (25 cells counted per condition for each experiment).

Bar: 10 μm.

Source data for plots and graphs are available online.